

# Analysis of the blowout plasma wakefields produced by drive beams with elliptical symmetry

P. Manwani,\* Y. Kang, J. Mann, B. Naranjo, G. Andonian, and J. B. Rosenzweig  
*Department of Physics and Astronomy, UCLA, Los Angeles, California 90095, USA*  
 (Dated: November 12, 2024)

In the underdense or blowout regime of plasma wakefield acceleration, the particle beam is denser than the plasma. Under these conditions, the plasma electrons are nearly completely rarefied from the beam channel, resulting in a nominally uniform ion column. Extensive investigations of this interaction assuming axisymmetry have been undertaken. However, the blowout produced by a transversely asymmetric driver, which would be present in linear collider "afterburner" scenarios, possesses quite different characteristics. Such beams create an asymmetric plasma rarefaction region which leads to asymmetric focusing in the two transverse planes, accompanied by a non-uniform accelerating gradient. The asymmetric blowout cross-section is found through simulation to be elliptical, and treating it as such permits simple extension of the symmetric theory. In particular, focusing fields which are linear in both transverse directions exist in the bubble. The form of the wake potential and the associated beam matching conditions in this elliptical cavity are discussed. We also discuss blowout boundary estimation in the long driver limit and applications of the salient asymmetric features of the wakefield.

Plasma wakefield acceleration (PWFA) is a key emerging technique for high energy accelerator applications such as colliders and X-ray free-electron lasers. The PWFA operates in two main regimes: linear [1] and non-linear (blowout) [2, 3]. In the blowout case, where the beam density  $n_b$  greatly exceeds the nominal plasma density  $n_0$ , the strong electric fields of the driver expel the plasma electrons outward, creating a blowout cavity (or bubble) entirely devoid of electrons. The expelled electrons and the electrons within a plasma skin depth of the boundary form a dense electron sheath which envelops the cavity. This plasma electron density and the associated return current shield the drive beam's electromagnetic fields outside of the bubble region [2, 4, 5]. The forces acting on the beam inside of the bubble are quite ideal for high quality acceleration, with no dependence of longitudinal forces on transverse offset. Further, the electrons undergo linear, aberration-free focusing dependent only on radial offset.

While axisymmetric driver scenarios have been extensively studied (see also, *e.g.* [6] and [7]), there are still many open questions to explore in the physics of plasma structures formed by strongly asymmetric drivers [8]. These scenarios are of critical importance in TeV-scale linear collider scenarios such as the so-termed *afterburner* [9]. The blowout created by these asymmetric, or flat, beams has been observed in simulations to be well-approximated by an elliptical cross-sectional form. Subsequently, the potential inside these elliptical cavities, which are translating at nearly the speed of light (beam velocity  $v_b \simeq c$ , depends quadratically on transverse coordinates, yielding linear transverse electric fields [10, 11]. To proceed with the analysis of this scenario, we use the three-dimensional particle-in-cell (PIC) code

OSIRIS [12] to investigate the electromagnetic fields inside the elliptical blowout cavity. We then employ these phenomenological results to guide development of a theoretical model.

Throughout this letter we use normalized units, where densities are normalized to  $n_0$ , which in turn specifies the characteristic oscillation frequency of the plasma electrons, the electron plasma frequency  $\omega_p = \sqrt{n_0 e^2 / m_e \epsilon_0}$ . This unitless notation is implemented as follows: time is normalized to  $\omega_p^{-1}$ ; velocities to the speed of light  $c$ ; masses to the electron mass  $m_e$ ; distance to the plasma skin-depth  $k_p^{-1} = c/\omega_p$ ; charge to the elementary charge  $e$ ; and electromagnetic field amplitudes to the so-termed wave-breaking [13] value  $m_e c \omega_p / e$ . There are source terms in our model and their species is indicated using the following subscripts: the plasma ions (i), the plasma electrons (e), and the drive beam (b).

To simplify our analysis, we make the common assumption that the more massive ions are static, forming a uniform background charge of  $n_i = 1$ . This assumption holds when the focusing phase advance of the ions is small,  $\Delta\phi = \sigma_z \sqrt{\pi Z_i n_b / m_i} \ll 1$ , where  $Z_i$  is the ionization state of the ions,  $m_i$  is the mass of the ions, and  $\sigma_z$  is the beam bunch length [14]. The source terms are then given as follows: the charge density  $\rho = \rho_b + \rho_e + 1$  and the current density  $\mathbf{J} = \mathbf{J}_b + \mathbf{J}_e$ . The equations of motion for the plasma electrons can be written in Hamiltonian form by introducing the vector and scalar potentials  $\mathbf{A}$  and  $\phi$ , and the canonical momenta  $\mathbf{P} = \mathbf{p} + \mathbf{A}$ . The beam evolution occurs on a much larger time-scale than the evolution of the plasma wakefield in the co-moving frame, thus permitting use of the quasi-static approximation  $(x, y, z, t) \rightarrow (x, y, \xi \equiv t - z, s \equiv z)$  [15], where we describe a slowly-varying disturbance in  $s$ , quantified through derivatives as  $\partial_s \ll \partial_\xi$ .

Under this approximation, Maxwell's equations for the

\* pkmanwani@gmail.com

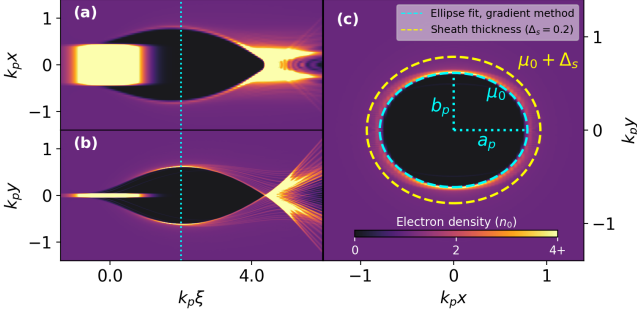


FIG. 1: Plasma wakefield created by a flat top driver with beam density  $n_b = 15$ , having asymmetric spot sizes:  $a = 0.424$ ,  $b = 0.0424$ . The longitudinal slices in the X-Z plane (a) and Y-Z plane (b), the transverse slice showing the elliptical profile (c).

normalized potentials in the Lorentz gauge reduce to

$$\nabla_{\perp}^2 \begin{bmatrix} \phi \\ \mathbf{A} \end{bmatrix} = - \begin{bmatrix} \rho \\ \mathbf{J} \end{bmatrix}, \quad (1)$$

where  $\nabla_{\perp}^2 = \partial_x^2 + \partial_y^2$  is the transverse Laplace operator. The Lorentz gauge condition  $\nabla \cdot \mathbf{A} + \frac{\partial \phi}{\partial t} = 0$  can now be written as  $\nabla_{\perp} \cdot \mathbf{A}_{\perp} = -\frac{\partial}{\partial \xi}(\phi - A_z) = -\frac{\partial}{\partial \xi}\psi$ . Here,  $\psi = \phi - A_z$  is the wake potential, or quasi-potential, which obeys the transverse Poisson equation  $-\nabla_{\perp}^2 \psi = \rho - J_z = S$ , where we define the source density as  $S$ . The continuity equation in the co-moving coordinate can be written as  $\frac{\partial}{\partial \xi} S + \nabla_{\perp} \cdot \mathbf{J}_{\perp} = 0$ . In this case, the Hamiltonian is given by  $H = \gamma - \phi$  with the Lorentz factor  $\gamma = \sqrt{1 + |\mathbf{p}|^2}$ . In the quasi-static approximation, the Hamiltonian depends on  $z$  and  $t$  only in the combination  $\xi = t - z$ . Hamilton's equations lead to the conservation of the quantity  $H - P_z$  via:  $\frac{dH}{dt} = \frac{\partial H}{\partial t} = \frac{\partial H}{\partial \xi} = -\frac{\partial H}{\partial z} = \frac{dP_z}{dt}$ . If the electrons are initially at rest, this implies,  $\gamma - \phi - p_z + A_z = 1$  [16, 17]. After substituting for the wake potential, this equation reduces to:

$$\gamma - \psi - p_z = 1 \quad (2)$$

The electromagnetic fields are found from the potentials:

$$\begin{aligned} E_z &= \frac{\partial \psi}{\partial \xi}; \quad \mathbf{E}_{\perp} = -\nabla_{\perp} \phi - \frac{\partial \mathbf{A}_{\perp}}{\partial \xi}; \\ \mathbf{B}_{\perp} &= \nabla_{\perp} \times \mathbf{A}_z + \nabla_z \times \mathbf{A}_{\perp}; \quad B_z = \nabla_{\perp} \times \mathbf{A}_{\perp} \end{aligned} \quad (3)$$

Note that when one considers forces on the beam in the ultra-relativistic beam limit  $v_b = c$  they are all simply derived from  $\psi$ . Here we are concentrating on the plasma response instead of the beam, and so the scenario of interest is more complex. Indeed, when the driver interacts with an underdense plasma, plasma electrons are strongly repelled by the first-order Coulomb force due to the beam charge, with magnetic effects becoming important for a relativistic plasma response, as is found in the blowout regime. This repulsion leads to strong,

non-laminar plasma motion, which upon evacuation of the plasma electrons from the beam channel ultimately leads to the formation of a blowout sheath surrounding a plasma-electron-free cavity.

To attain a preliminary understanding of this system in the case of an asymmetric drive beam, we first consult the results of electromagnetic PIC simulations (see Figure 1, which shows the output from the code OSIRIS [12]). When considering a transversely elliptical-shaped drive beam, the blowout cavity and sheath (the cavity boundary) also take on elliptical shapes in cross-section. The transverse asymmetry of the wakefield produced by the asymmetric beam can be seen in the longitudinal slices shown in Figure 1. The asymmetry drives sheath electron trajectories behind the blowout in a more complex manner, contrasting with the symmetric case where the simultaneous crossing of trajectories results in a large near-axis density spike. The transverse slice of the wakefield itself shows the elliptical cross-section created by the evacuated plasma electrons, having semi-axes  $a_p$  and  $b_p$  and a thin, dense plasma electron sheath of width  $\Delta_p$ . There is also a longitudinal plasma return current outside the ion bubble within a thickness near  $k_p^{-1}$ , *i.e.*  $\Delta_j \approx 1$ . For the ease of this analysis, we treat the source sheath thickness,  $\Delta_s$ , to be the same as the plasma density sheath thickness,  $\Delta_p$ , as  $\rho - J_z \approx \rho$  [5]. We assume the density of this sheath to be uniform and the thickness to be confocal with the ion column ellipse. The confocal condition stems from our choice of a uniform density distribution that does not vary with the angular coordinate. This choice was made because of its simplicity and alignment with observations. However, the confocal condition can be extended to other distributions that more closely match the exponential spatial decay of the sheath layer observed in PIC simulations. We show in the Appendix that this confocal condition allows us to construct a solution for the wake potential that vanishes outside the sheath, which is a direct consequence of the assumption that no electromagnetic fields exist outside the electron sheath.

We can integrate the charge continuity relation over the transverse plane, and with the divergence theorem we attain the conservation of the sources through each transverse plane,  $\frac{d}{d\xi} \int S dA = 0$ . With the absence of any source ahead of the driver, this conservation results in net zero source on each transverse plane,  $\int S dA = 0$ , allowing us to determine the sheath density. We now introduce elliptical coordinates  $(\mu, \nu)$  using the substitution  $x = c_p \cosh \mu \cos \nu$  and  $y = c_p \cosh \mu \sin \nu$ , with  $\mu_0$  and  $c_p = \sqrt{a_p^2 - b_p^2}$  defining the elliptical blowout boundary and focal length of the ellipse, respectively. The sheath is confocal to the ellipse defined by  $\mu_0$ . We can now construct the Poisson equation with the defined source terms

for each transverse slice:

$$-\nabla_{\perp}^2 \psi = -\frac{2}{c_p^2(\cosh 2\mu - \cos 2\nu)} \left( \frac{\partial^2 \psi}{\partial \mu^2} + \frac{\partial^2 \psi}{\partial \nu^2} \right) \\ = \begin{cases} 1 & \mu < \mu_0, \\ -\frac{\sinh 2\mu_0}{\sinh(2\mu_0 + 2\Delta_s) - \sinh 2\mu_0} & \mu_0 < \mu < \mu_0 + \Delta_s, \\ 0 & \mu > \mu_0 + \Delta_s. \end{cases} \quad (4)$$

Here, we assume that  $\Delta_s$  is small compared to  $\mu_0$ . We are interested in the solution of the wake potential inside the ellipse, and so we can expand the equation up to first order in  $\Delta_s$ :

$$\psi|_{\mu < \mu_0} = -\frac{c_p^2}{8} \left[ \cosh 2\mu - \cosh 2\mu_0 + \left( 1 - \frac{\cosh 2\mu}{\cosh 2\mu_0} \right) \cos 2\nu \right. \\ \left. + \Delta_s \left( \sinh 2\mu_0 - \tanh 2\mu_0 \frac{\cosh 2\mu}{\cosh 2\mu_0} \cos 2\nu \right) \right] \quad (5)$$

Converting the results to Cartesian coordinates using  $x = c \cosh \mu \cos \nu$  and  $y = c \sinh \mu \sin \nu$ , we find

$$\psi(x, y) = -\frac{x^2 b_p^2 + y^2 a_p^2 - p_p^4}{2d_p^2} \\ - \frac{\Delta_s p_p^2}{2d_p^4} \left[ (x^2 - y^2) c_p^2 - a_p^4 - b_p^4 \right], \quad (6)$$

where  $p_p^2 = a_p b_p$  and  $d_p^2 = a_p^2 + b_p^2$ . We note that this wake potential, which determines the motion of ultra-relativistic electrons within the blowout cavity, is quadratic in both  $x$  and  $y$ . As this potential is that of a two-dimensional simple-harmonic oscillator, focal characteristics and therefore matched (equilibrium propagation) beam conditions in both transverse planes can be derived from Eq. 6.

In general, the wakefields can be derived from the gradient of the wake potential, as:

$$W_x = E_x - B_y = -\frac{\partial \psi}{\partial x} = x \left[ \frac{b_p^2}{d_p^2} + \Delta_s \frac{p_p^2 c_p^2}{d_p^4} \right] \\ W_y = E_y + B_x = -\frac{\partial \psi}{\partial y} = y \left[ \frac{a_p^2}{d_p^2} - \Delta_s \frac{p_p^2 c_p^2}{d_p^4} \right] \quad (7) \\ W_z = E_{z,p} = \frac{\partial \psi}{\partial \xi} = \frac{p^2}{d^4} \left[ C_1(x^2 - y^2) + C_2 \right] \\ + \frac{\Delta \mu}{2d^6} \left[ C_3(x^2 - y^2) + C_4 \right]$$

where ' indicates the derivative with respect to  $\xi$ ,  $C_1 = a_p' b_p - b_p' a_p$ ,  $C_2 = a_p' b_p^3 + b_p' a_p^3$ ,  $C_3 = C_1(a_p^4 - 6a_p^2 b_p^2 + b_p^4)$ , and  $C_4 = (a_p^6 + b_p^6)(p_p^2)' + (a_p^5)' b_p^3 - a_p^5 (b_p^3)' + a_p^3 (b_p^5)' - (a_p^3)' b_p^5$ . We can estimate the physical size of the sheath thickness in the two transverse planes by switching back

to Cartesian coordinates, *i.e.*  $\Delta_x \approx b_p \Delta_s$  and  $\Delta_y \approx a_p \Delta_s$ . Note the linearity of the transverse wakefields in their respective coordinates.

Our simulations indicate that a thin sheath,  $\Delta_s \lesssim 0.2$ , yields reasonable results for the transverse wakefields, so the electron sheath can be further approximated as infinitesimally thin ( $\Delta_s \rightarrow 0$ ). We may then proceed without using an external fitting parameter, as was done in Ref. [18]. Additionally, as we assume that no electromagnetic fields exist outside the blowout due to the shielding provided by the sheath at  $\partial\Omega(\xi)$  (the boundary of the blowout area  $\Omega(\xi)$ ), we may set  $\psi$  to be zero everywhere outside the blowout region. This allows us to write:  $\nabla_{\perp}^2 \psi(\xi) = -1$ , with  $\psi|_{\partial\Omega(\xi)} = 0$ , providing the same result as above without the sheath thickness parameter:  $\psi = -(x^2 b_p^2 + y^2 a_p^2 - p_p^4)/2d_p^2$ . In the axisymmetric limit,  $a_p = b_p$ , and we attain the standard result  $\psi_r = -(r^2 - r_b^2)/4$ , where  $r$  is the radial coordinate and  $r_b$  is the blowout radius.

We verify our approach by comparing the output the PIC simulations with these analytical results. The axes of the resulting ellipse can be found by numerically evaluating the boundary positions via a least-squares fitting of select boundary points marking the position maximum gradient of density for 100 radially-directed line searches taken at uniformly spaced angles. The relative root mean square error (RRMSE) between the PIC-simulated transverse fields and the fields predicted by Equation 7 (with geometry found via the elliptical fit to the boundary points) is shown in Figure 2. The RRMSE is calculated by considering each data point within the blowout boundary,  $\text{RRMSE} = \sqrt{\frac{1}{n} \sum_{i=1}^n (X_i - \hat{X}_i)^2 / (\frac{1}{n} \sum_{i=1}^n \hat{X}_i^2)}$ , with  $X_i$  representing the analytical fields and  $\hat{X}_i$  representing the PIC-simulated fields. Our elliptical model's predictions for transverse wakes closely match simulations, additionally showing that sheath thickness varies with driver strength.

While this is not a main thrust of the current work, a few comments on the longitudinal wake  $W_z$  are relevant here. The Panofsky-Wenzel theorem [19], as applied to plasma wakefields is  $\nabla_{\perp} W_z = \partial_{\xi} W_{\perp}$ . This follows from their description in terms of a unique potential  $\psi$ . In the case of a symmetric blowout,  $W_z$  has been long known to be independent of  $x$  and  $y$  as a result of the constant nature of  $W_{\perp}$  after blowout, and is independent of the sheath thickness due to the axisymmetrical shape of the wakefield. However, with the elliptical shape of the bubble,  $W_z$  becomes coordinate dependent and varies with the sheath thickness. A larger thickness,  $\Delta_s \approx 0.6$ , yields better results for the longitudinal wakefield. This disparity in the sheath dependence of the wakefields likely arises from the specific shape of the  $\rho$  and  $J_z$  distributions, and will need to be investigated in the future.

We now move to the estimation of the elliptical boundaries using the beam parameters in the long beam limit,  $k_p \sigma_z \gg 1$ , neglecting the longitudinal variation of the fields near the axial center of the beam ( $\partial_{\xi} \ll \partial_{\perp}$ ). We

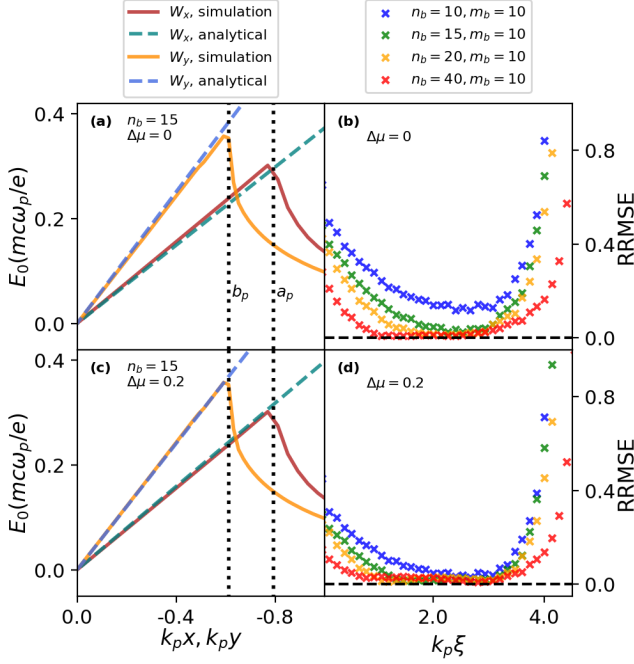


FIG. 2: Short beam ( $\sigma_z = 0.5$ ) driver, corresponding to the case of Fig. 1. (a) Transverse wakefield line-outs of the wake. (b) Comparison between the analytical transverse wakefield  $W_\perp$  from different  $n_b$ , calculated using the fitted blowout boundary.

can obtain the force on the plasma electrons at a position near the sheath,  $\mathbf{r}$ , by considering the plasma electron's transverse velocity  $\mathbf{v}_\perp = d\mathbf{r}_\perp/dt = (1 - v_z) d\mathbf{r}_\perp/d\xi = \gamma^{-1}(1 + \psi) d\mathbf{r}_\perp/d\xi$  in combination with Eq. 2,

$$\mathbf{F}_\perp = (1 - v_z) \frac{d\mathbf{p}_\perp}{d\xi} = \frac{1}{\gamma} (1 + \psi) \frac{d}{d\xi} \left( (1 + \psi) \frac{d}{d\xi} \mathbf{r}_\perp \right) \quad (8)$$

$$\mathbf{F}_\perp|_{\partial\Omega} = \frac{1}{\gamma} \left( \frac{d\psi}{d\xi} \frac{d\mathbf{r}_\perp}{d\xi} + \frac{d^2\mathbf{r}_\perp}{d\xi^2} \right) \Big|_{\partial\Omega} = 0. \quad (9)$$

Neglecting variations along  $\xi$  allows us to balance the transverse forces at the boundaries. We additionally assume that the plasma electron longitudinal velocity  $v_z$  does not depend on the transverse coordinate. This facilitates the solution to the above equations by providing a linear relationship between  $\phi_e$  and  $A_e$ , to which we can add  $v_z$  effects as a correction. Using Eq. 3 to convert to a potential description and assuming  $v_b = 1$ :

$$\mathbf{F}_\perp = \nabla_\perp \phi_i + \nabla_\perp \phi_e + \nabla_\perp \phi_b + \partial_\xi \mathbf{A}_\perp - (\nabla_\perp \mathbf{A}) \cdot \mathbf{v} - (\mathbf{v} \cdot \nabla) \mathbf{A}_\perp \quad (10)$$

With Eq. 9 and neglecting the longitudinal variation of the transverse velocity and fields leads to the relation:

$$(1 + v_z) \nabla_\perp \psi|_{\partial\Omega} - v_z \nabla_\perp \phi_i|_{\partial\Omega} + (1 - v_z) \nabla_\perp \phi_b|_{\partial\Omega} = 0 \quad (11)$$

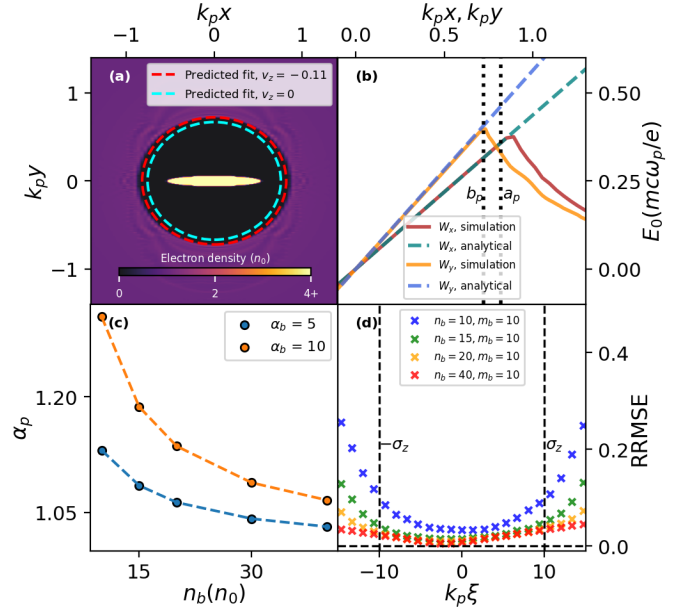


FIG. 3: Long beam ( $\sigma_z = 10$ ) driver: (a) Analytical calculation for the blowout shape using a beam with  $n_b = 20$ ,  $a = 0.5$  and  $b = 0.05$ . (b) Transverse wakefield lineouts of the wake, calculated using the predicted blowout boundary. (c) predicted blowout ellipticity at the center of wake vs beam density and beam ellipticity. (d) Comparison between the analytically calculated transverse wakefield and the simulation results.

Since the cavity is nearly completely evacuated of plasma electrons, we can obtain the scalar potential due to the remaining ions,  $\phi_i(\xi) = -\frac{x^2 b_p(\xi) + y^2 a_p(\xi)}{2(a_p(\xi) + b_p(\xi))}$  [20]. We neglect  $v_z$  to get the zero-th order equation in the electrostatic limit. Using Ampere's law in integral form,  $\oint \mathbf{B} \cdot d\mathbf{l} = \int (\mathbf{J} + \epsilon_0 \frac{\partial \mathbf{E}}{\partial t}) \cdot d\mathbf{a}$ , we can integrate over the transverse plane to remove the left hand side term to get  $I_{z,beam} + I_{z,elec} + \int_0^\infty \frac{\partial^2 \psi}{\partial \xi^2} da = 0$ . In the limit of a long beam, the integral term becomes negligible. Consequently, this verifies the equivalence between the return beam current and the plasma return current layer of thickness  $\Delta_j = 1$ . By assuming the longitudinal velocity  $v_z$  to be constant across this region area, we find that  $v_z = \frac{\lambda_b}{\pi(a_p+1)(b_p+1)}$ , where  $\lambda_b$  is the beam charge per unit length. This enables us to re-incorporate electromagnetic features of the sheath, beyond the zero-th order analysis above, in weak blowout scenarios. However, for highly nonlinear blowouts, a comprehensive treatment of the wakefields becomes important. Fortunately, in this limit, axisymmetry is inherently approached and additional treatment of the higher order moments is not essential. We use the electric fields of the elliptical drive beam [21] to simultaneously find  $\psi$  and the elliptical semi-axes  $a_p$  and  $b_p$  such that the transverse forces on the ellipse boundaries are minimized. Here  $\alpha_p = a_p/b_p$  represents the ellipticity of the plasma blowout. We verify our results by calculating the blowout shape for a long

beam driver, predicting the transverse fields and calculating the RRMSE values in Fig. 3 (see Supplemental Material for the details on PIC simulations [22]).

The equations that govern the transverse beam dynamics inside the blowout cavity are:

$$x''(z) + K_x x(z) = 0; \quad y''(z) + K_y y(z) = 0 \quad (12)$$

$$K_x = K_r \frac{2}{1 + \alpha_p^2}; \quad K_y = K_r \frac{2\alpha_p^2}{1 + \alpha_p^2} \quad (13)$$

where  $K_r = n_p/2\gamma$  arises from the linear focusing strength of the ions in an axisymmetric ion column and  $n_p$  represents the normalized plasma density. The matching conditions of a beam propagating in this blowout cavity are then given as:

$$\sigma_{m,\eta} = \sqrt{\frac{\sqrt{K_\eta^{-1}} \epsilon_{n,\eta}}{\gamma}} \rightarrow \frac{\sigma_{m,x}}{\sigma_{m,y}} = \sqrt{\frac{\epsilon_{n,x}}{\epsilon_{n,y}}} \alpha_p \quad (14)$$

where  $\eta \in \{x, y\}$  and  $\epsilon_{n,\eta}$  are the normalized emittances, where the aspect ratio of the matched beam is now determined by the combination of the emittance ratio and the ellipticity of the wake. This condition can be used to match the beam inside a given plasma profile.

In this paper, we have created a phenomenological model for understanding the structure of plasma columns formed by elliptical beams, which is crucial as it dictates the focusing forces of the wakefield, thus influencing beam dynamics significantly. This comprehension is essential for plasma wakefield experiments and scenarios involving plasma afterburners utilizing asymmetric beams. The findings presented herein shed light on the ellipticity and emittance requirements for achieving beam matching within the elliptical blowout cavity [23]. This approach can also be utilized in the context of laser wakefield acceleration (LWFA) [24], but care must be taken to distinguish the asymmetry in the drivers due to the local nature of the ponderomotive force compared with the global nature of the Coulombic interaction. The disparity in focusing forces in the two transverse planes presents unique challenges and opportunities. These include a plasma wakefield experiment planned at the Argonne Wakefield Accelerator (AWA), that would study the propagation of a particle beam in a plasma with asymmetric transverse emittances [25–27], as well as the development of an asymmetric plasma lens using the asymmetry in the focal lengths, which will be detailed in a subsequent paper [28]. We have listed additional comparisons in the Supplemental Material [22] and have done a comparison study on the shape of the elliptical blowout between Gaussian and flat-top beams [29]. While this paper lays the foundation, further research is necessary to fully characterize asymmetric wakefields as was done for axisymmetric beams in

[4, 18] and ongoing efforts aim to generalize properties of this asymmetric beam-plasma interaction.

The authors would like to thank Nathan Majernik for insightful discussions. This work was performed with the support of the US Department of Energy under Contract No. DE-SC0017648 and DE-SC0009914. This work used resources of the National Energy Research Scientific Computing Center (NERSC), a U.S. DOE Office of Science User Facility, operated under Contract No. DE-AC02-05CH11231.

## I. APPENDIX

We start with the analysis done by Regenstreif to find the potential and field produced by a uniform beam with charge density  $\rho$  inside a confocal vacuum chamber[30]. We define two boundaries: one for the vacuum chamber and one for the beam, respectively  $\mu = \mu_1$  and  $\mu = \mu_0$ .

$$\begin{aligned} \psi_{\mu > \mu_0} &= \frac{\rho c_p^2}{8} \left[ 2(\mu_1 - \mu) - \frac{\sinh 2(\mu_1 - \mu)}{\cosh 2\mu_1} \cos 2\nu \right] \sinh 2\mu_0 \\ \psi_{\mu < \mu_0} &= \frac{\rho c_p^2}{8} \left( \left[ \frac{\cosh 2(\mu_1 - \mu_0)}{\cosh 2\mu_1} \cosh 2\mu - 1 \right] \cos 2\nu \right. \\ &\quad \left. + \cosh 2\mu_0 - \cosh 2\mu + 2(\mu_1 - \mu_0) \sinh 2\mu_0 \right) \end{aligned} \quad (A1)$$

Taking the chamber to be at infinity,  $\mu_1 \rightarrow \infty$ , we have the substitutions  $\lim_{\mu_1 \rightarrow \infty} \frac{\sinh(2\mu_1 - 2\mu)}{\cosh 2\mu_1} = \cosh 2\mu - \sinh 2\mu$  and  $\lim_{\mu_1 \rightarrow \infty} \frac{\cosh(2\mu_1 - 2\mu_0)}{\cosh 2\mu_1} = \cosh 2\mu_0 - \sinh 2\mu_0$ . Ignoring the constant term that contributes to infinity, a solution for the isolated beam can be obtained:

$$\begin{aligned} \psi_{\mu > \mu_0} &= -\frac{\rho c_p^2}{8} [2\mu + (\cosh 2\mu - \sinh 2\mu) \cos 2\nu] \sinh 2\mu_0 \\ \psi_{\mu < \mu_0} &= -\frac{\rho c_p^2}{8} \left( [1 - (\cosh 2\mu_0 - \sinh 2\mu_0) \cosh 2\mu] \cos 2\nu \right. \\ &\quad \left. + \cosh 2\mu_0 - \cosh 2\mu - 2\mu_0 \sinh 2\mu_0 \right) \end{aligned} \quad (A2)$$

We can use this analysis, to construct the source term,  $S = \rho - J_z$  by using two confocal ellipses overlapping each other;  $\mu_{in} = \mu_0$  and  $\mu_{out} = \mu_0 + \Delta_s$ . To yield the desired source distribution defined in the paper, we set the source densities to be  $S_{in} = -S_{\Delta_s}$  and  $S_{out} = \rho_i + S_{\Delta_s}$ . Applying the conservation of  $S$  in the transverse plane,  $\int_0^{2\pi} \int_0^{\mu_{out}} (S_{in} + S_{out}) \frac{c_p^2}{2} (\cosh 2\mu - \cos 2\nu) d\mu d\nu = 0$ , yielding:

$$S_{\Delta_s} = -\frac{\rho_i \sinh(\mu_0 + \Delta_s)}{\sinh(\mu_0 + \Delta_s) - \sinh \mu_0} \quad (A3)$$

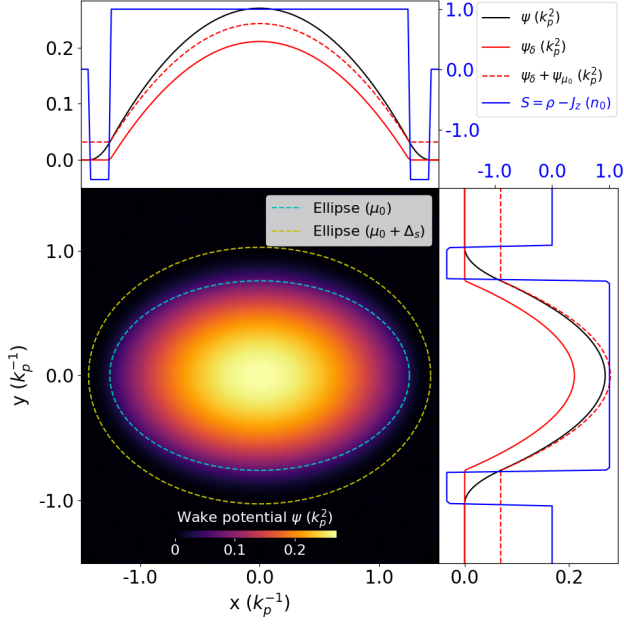


FIG. A1: Wake potential calculated for a specific set of parameters ( $c_p = 1$ ,  $\mu_0 = 0.7$ ,  $\Delta_s = 0.2$ ). The plot illustrates the shape of the wake potential  $\psi$  with the corresponding line-outs along the  $x$  and  $y$  axes. It also includes the line-outs of the source term  $S$  and the delta-function potential  $\psi_\delta$ .

We now have the complete form of the source density and can find the  $\psi$  using the superposition of the wake potentials of the two confocal ellipses. The combination of the conservation of the source term and the confocality condition has a key property: outside the sheath, the wakefield due to the sheath cancels out the wakefield due to the ion column, i.e.  $\psi|_{\mu > \mu_0} = 0$ . The confocal model works well to capture this essential quality of the blowout regime, showing the elliptical symmetry of the fields. We are also interested in the form of  $\psi$  inside the ion column to calculate the wakefields, and inside the sheath to calculate the electron trajectories. This can be calculated from the isolated beam solutions.

Here, we simplify the former by introducing the assumption that the sheath thickness is small compared to

the ion column ( $\Delta_s/\mu_0 < 1$ ), yielding the solutions (up to first order in  $\Delta_s$ ):

$$\psi|_{\mu < \mu_0} = -\frac{c_p^2}{8} \left[ \cosh 2\mu - \cosh 2\mu_0 + \left( 1 - \frac{\cosh 2\mu}{\cosh 2\mu_0} \right) \cos 2\nu \right] + \Delta_s \left( \sinh 2\mu_0 - \tanh 2\mu_0 \frac{\cosh 2\mu}{\cosh 2\mu_0} \cos 2\nu \right) \quad (\text{A4})$$

If we assume the sheath to be infinitesimal ( $\Delta_s \rightarrow 0$ ), there is an alternative method that can be used to arrive at the same solution. Assuming no electromagnetic fields exist outside the blowout due to the shielding provided by the sheath at  $\partial\Omega(\xi)$ , we may then set the wake potential to be zero everywhere outside the blowout region. Finally, the constant charge density inside the cavity from the ions alone enables us to solve for the wake. In this case, we have:  $\nabla_\perp^2 \psi_\delta(\xi) = -1$ , with  $\psi_\delta|_{\partial\Omega(\xi)} = 0$ . In this case, the particular solution is:

$$\psi_{\delta,p} = -\frac{a^2}{8} (\cosh(2\mu) - \cosh(2\mu_0) + \cos(2\nu)) \quad (\text{A5})$$

We add a homogeneous solution such that potential is 0 at  $\mu = \mu_0$ :

$$\psi_{\delta,h} = \frac{a^2}{8} \left( \frac{\cosh(2\mu)}{\cosh(2\mu_0)} \right) \cos(2\nu) \quad (\text{A6})$$

Adding the particular and homogenous solutions gives us the same result as  $\lim_{\Delta_s \rightarrow 0} \psi = \psi_\delta$

$$\psi_\delta = -\frac{c_p^2}{8} \left( \cosh 2\mu - \cosh 2\mu_0 + \left( 1 - \frac{\cosh 2\mu}{\cosh 2\mu_0} \right) \cos 2\nu \right) \quad (\text{A7})$$

The exact wake potential solution including the sheath, along with the solution from the delta function approximation is shown in Fig. A1. Adding an offset to the delta function approximation allows us to study the differences between the two wake potential profiles. This comparison is crucial for analyzing the gradients (wakefields), which are of primary interest in our study.

- 
- [1] P. Chen, J. M. Dawson, R. W. Huff, and T. Katsouleas, Acceleration of electrons by the interaction of a bunched electron beam with a plasma, *Phys. Rev. Lett.* **54**, 693 (1985).
  - [2] J. B. Rosenzweig, B. Breizman, T. Katsouleas, and J. J. Su, Acceleration and focusing of electrons in two-dimensional nonlinear plasma wake fields, *Phys. Rev. A* **44**, R6189 (1991).
  - [3] N. Barov, J. B. Rosenzweig, M. E. Conde, W. Gai, and J. G. Power, Observation of plasma wakefield accel-

- ation in the underdense regime, *Phys. Rev. ST Accel. Beams* **3**, 011301 (2000).
- [4] W. Lu, C. Huang, M. Zhou, W. B. Mori, and T. Katsouleas, Nonlinear theory for relativistic plasma wakefields in the blowout regime, *Phys. Rev. Lett.* **96**, 165002 (2006).
- [5] S. A. Yi, V. Khudik, C. Siemon, and G. Shvets, Analytic model of electromagnetic fields around a plasma bubble in the blow-out regime, *Physics of Plasmas* **20**, 013108 (2013), <https://pubs.aip.org/aip/pop/article->

- pdf/doi/10.1063/1.4775774/13429408/013108\_1.online.pdf.
- [6] N. Barov, J. B. Rosenzweig, M. C. Thompson, and R. B. Yoder, Energy loss of a high-charge bunched electron beam in plasma: Analysis, *Phys. Rev. ST Accel. Beams* **7**, 061301 (2004).
  - [7] J. B. Rosenzweig, N. Barov, M. C. Thompson, and R. B. Yoder, Energy loss of a high charge bunched electron beam in plasma: Simulations, scaling, and accelerating wakefields, *Phys. Rev. ST Accel. Beams* **7**, 061302 (2004).
  - [8] S. S. Baturin, Flat bubble regime and laminar plasma flow in a plasma wakefield accelerator, *Phys. Rev. Accel. Beams* **25**, 081301 (2022).
  - [9] D. J. Harris, Building accelerator afterburners with plasma, *proceedings of the National Academy of Sciences* **113**, 1107 (2016).
  - [10] P. Manwani *et al.*, Beam Matching in an Elliptical Plasma Blowout Driven by Highly Asymmetric Flat Beams, in *Proc. IPAC'22*, International Particle Accelerator Conference No. 13 (JACoW Publishing, Geneva, Switzerland, 2022) pp. 1802–1805.
  - [11] P. Manwani, N. Majernik, J. Mann, Y. Kang, D. Chow, H. Ancelin, G. Andonian, and J. Rosenzweig, Flat beam plasma wakefield accelerator (2023), [arXiv:2305.01902](https://arxiv.org/abs/2305.01902) [physics.acc-ph].
  - [12] R. A. Fonseca, S. F. Martins, L. O. Silva, J. W. Tonge, F. S. Tsung, and W. B. Mori, One-to-one direct modeling of experiments and astrophysical scenarios: pushing the envelope on kinetic plasma simulations, *Plasma Physics and Controlled Fusion* **50**, 124034 (2008).
  - [13] J. M. Dawson, Nonlinear electron oscillations in a cold plasma, *Phys. Rev.* **113**, 383 (1959).
  - [14] J. B. Rosenzweig, A. M. Cook, A. Scott, M. C. Thompson, and R. B. Yoder, Effects of ion motion in intense beam-driven plasma wakefield accelerators, *Phys. Rev. Lett.* **95**, 195002 (2005).
  - [15] P. Sprangle, E. Esarey, and A. Ting, Nonlinear interaction of intense laser pulses in plasmas, *Phys. Rev. A* **41**, 4463 (1990).
  - [16] P. Mora and T. M. Antonsen, Jr., Kinetic modeling of intense, short laser pulses propagating in tenuous plasmas, *Physics of Plasmas* **4**, 217 (1997), [https://pubs.aip.org/aip/pop/article-pdf/4/1/217/12532941/217\\_1.online.pdf](https://pubs.aip.org/aip/pop/article-pdf/4/1/217/12532941/217_1.online.pdf).
  - [17] W. Lu, C. Huang, M. Zhou, M. Tzoufras, F. S. Tsung, W. B. Mori, and T. Katsouleas, A nonlinear theory for multidimensional relativistic plasma wave wakefields, *Physics of Plasmas* **13**, 056709 (2006), [https://pubs.aip.org/aip/pop/article-pdf/doi/10.1063/1.2203364/15804477/056709\\_1.online.pdf](https://pubs.aip.org/aip/pop/article-pdf/doi/10.1063/1.2203364/15804477/056709_1.online.pdf).
  - [18] A. Golovanov, I. Y. Kostyukov, A. Pukhov, and V. Malka, Energy-conserving theory of the blowout regime of plasma wakefield, *Phys. Rev. Lett.* **130**, 105001 (2023).
  - [19] W. K. H. Panofsky and W. A. Wenzel, Some Considerations Concerning the Transverse Deflection of Charged Particles in Radio-Frequency Fields, *Review of Scientific Instruments* **27**, 967 (1956), [https://pubs.aip.org/aip/rsi/article-pdf/27/11/967/19098135/967\\_1.online.pdf](https://pubs.aip.org/aip/rsi/article-pdf/27/11/967/19098135/967_1.online.pdf).
  - [20] M. R. Shubaly, Space charge fields of elliptically symmetrical beams, *Nuclear Instruments and Methods* **130**, 19 (1975).
  - [21] G. Parzen, Electric fields of a uniformly charged elliptical beam (2001), [arXiv:physics/0108040](https://arxiv.org/abs/physics/0108040) [physics.acc-ph].
  - [22] See supplemental material at [url will be inserted by publisher] for details on pic simulations and computational methods.
  - [23] P. Manwani, A. Ody, D. Chow, G. Andonian, J. Rosenzweig, and Y. Kang, Flat beam transport for a PWFA experiment at AWA, in *Proc. IPAC'24*, International Particle Accelerator Conference No. 15 (JACoW Publishing, Geneva, Switzerland, 2024) pp. 580–582.
  - [24] T. Tajima and J. M. Dawson, Laser electron accelerator, *Phys. Rev. Lett.* **43**, 267 (1979).
  - [25] T. Xu, M. Conde, G. Ha, M. Kuriki, P. Piot, J. Power, and E. Wisniewski, Generation High-Charge of Flat Beams at the Argonne Wakefield Accelerator, in *10th International Particle Accelerator Conference* (2019).
  - [26] P. Manwani *et al.*, Asymmetric Beam Driven Plasma Wakefields at the AWA, in *Proc. IPAC'21* (JACoW Publishing, Geneva, Switzerland) pp. 1732–1735.
  - [27] M. Yadav *et al.*, Radiation Diagnostics for AWA and FACET-II Flat Beams in Plasma, in *Proc. IPAC'22*, International Particle Accelerator Conference No. 13 (JACoW Publishing, Geneva, Switzerland, 2022) pp. 1791–1794.
  - [28] Manwani *et al.*, Propagation of beams inside a transversely elliptical blowout plasma wakefield (2024), manuscript in preparation.
  - [29] Y. K. et al., Comparison of flat beam pwfa analytic model with pic simulations, in *Proc. IPAC'24*, IPAC'24 - 15th International Particle Accelerator Conference No. 15 (JACoW Publishing, Geneva, Switzerland, 2024) pp. 583–586.
  - [30] E. Regenstein, Potential and field produced by a uniform or non-uniform elliptical beam inside a confocal elliptic vacuum chamber, *IEEE Trans. Nucl. Sci.*; (United States) (1977).